J. Appl. Comput. Mech., 11(1) (2025) 143-159
DOI: 10.22055/jacm.2024.46199.4478

ISSN: 2383-4536
jacm.scu.ac.ir

Shahid Chamran University of Ahvaz

Journal of Applied and Computational Mechanics

Research Paper

Design Methodology of a Novel Comminution Machine

R.M.R. Panduro[1], A. Córdova[1], J.L. Mantari[2]

[1] Faculty of Mechanical Engineering, National University of Engineering, Av. Túpac Amaru 210, Lima, 15333, Perú,
Email: rpanduroc@uni.pe (R.M.R.P.); acordovar@uni.pe (A.C.)

[2] Department of Mechanical Engineering, Universidad de Ingeniería y Tecnología - UTEC, Jr. Medrano Silva 165, Barranco, Lima, Peru, Email: jmantari@utec.edu.pe

Received February 21 2024; Revised June 11 2024; Accepted for publication June 12 2024.
Corresponding author: J.L. Mantari (jmantari@utec.edu.pe)

Abstract. This paper outlines the conceptual and numerical design process of a comminution equipment centered on particle breakdown through impact. The process is divided into four stages, starting with the generation of device concepts achieved by developing a needs matrix for an optimal machine. Subsequently, in the second stage, various equipment shape proposals were introduced and tested, with the selection of an optimal proposal determined through performance comparisons. For comparison purposes, simulations utilizing the discrete element method (DEM) were conducted, considering analyses of accumulated power from collisions and particle breakage. Once the optimized prototype was identified, a breakage simulation was conducted to measure the device's reduction ratio. In the third stage, the machine elements of the device were calculated. Finally, in the fourth stage, a series of simulations utilizing the finite element method (FEM) were carried out to perform structural and modal analyses of the final design. The evaluated variables identified in the simulations played a crucial role in optimizing the design, ultimately resulting in a device with a reduction ratio of 1:19.8 for limestone.

Keywords: Comminution, Mining, Machine Design, DEM, FEM.

1. Introduction

The grinding and crushing processes are identified as the largest consumers of energy in mining comminution operations. Between 30 to 70% of the total energy consumption is attributed to comminution, with up to 50% specifically allocated to grinding [1]. This inefficiency underscores the need for process improvement. By exploring new technologies in the search for real innovation in comminution machines, there is potential to reduce energy consumption in comminution [2].

In the quest for innovative machinery, parametric analysis facilitates the systematic exploration of designs. Here, establishing decision rules and identifying the most critical parameters become genuinely crucial for optimizing designs. In the current literature, it is possible to find valuable tools employed in decision-making processes. For instance, in manufacturing processes, it is possible to find the application of Rough Sets Theory as a data mining tool [3] or the application of discriminant analysis [4]. Such applications simplify the identification of relationships between parameters and predict responses to various combinations of input parameters. Other tools, such as real-time analysis, offer information for prompt decision-making and response generation. Real-time monitoring applications are observable in reliable applications that streamline obtaining information [5]. Additionally, taking advantage of emerging disruptive technologies, such as machine learning or the Internet of Things, real-time analysis is used to facilitate the development of customized product design [6].

Computational mechanics methods play a fundamental role in developing innovative designs for grinding and crusher devices. Currently, the application of new techniques has the potential to enhance the utility of computational simulations. Modern advancements in geometry representation methods of microstructures can supply suitable input for computational fluid dynamics (CFD) simulations [7]. Likewise, numerical analyses can be validated and enhanced through the use of digital image correlation (DIC) techniques [8]. Recent studies provide insights into determining the appropriate speckle pattern for achieving accurate strain measurements [9] and even establishing the suitable speckle size if DIC analysis is conducted at a microscale [10]. Additionally, various methods exploring different numerical approaches are currently under development, such as the continuum-discontinuum element method (CDEM) to investigate hydraulic fracture propagation [11]. These examples illustrate how computational mechanics offers opportunities to overcome constraints and drive genuine innovation.

However, computational techniques must involve proper modeling of the comminution process, allowing fundamental understanding of particle behavior inside the devices, as well as the breakage of particles in the process [12]. Especially, if it is required to make predictions about the operation performance of these devices. Under this context, the discrete element method (DEM) emerges as the tool best suited for studying the operational environment of crushing devices, while also providing a suitable framework for model comparison.

Published online: June 23 2024

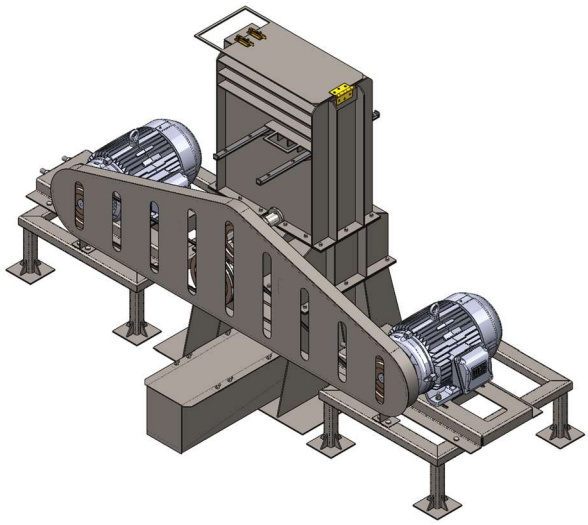

Fig. 1. Design of a novelty comminution machine.

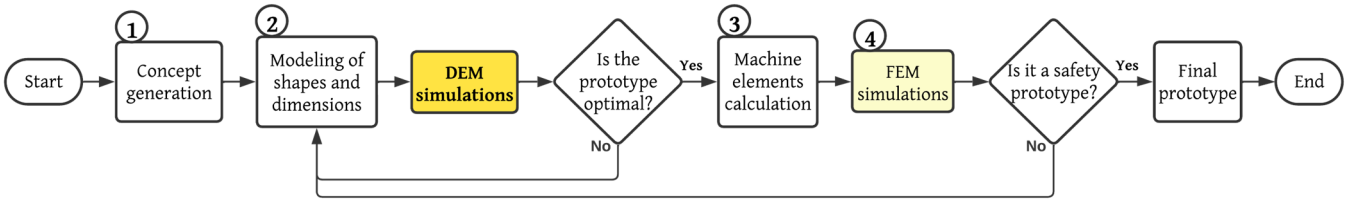

Fig. 2. Process flow diagram for design of novelty machine.

The discrete element method (DEM) is a numerical method based on the application of Newton's second law and contact models to solve forces acting on particles. Commonly used contact models are the Linear spring-dashpot model [13], Mindlin-Deresiewicz model [14], and Walton and Braun's model [15]. Computational simulations based on DEM provide a mechanistic approach to the environment inside comminution devices, where the chaotic environment can be described as a deterministic process on a particle scale [16]. Therefore, DEM is perfectly applicable to the study of crusher device performance. Since DEM was proposed by Cundall and Strack [13], several authors have supported DEM as a reliable and powerful tool to understand and model particle systems, as it is reviewed by Zhu et al. [17,16], Weerasekara et al. [18] and Tavares [19]. A great example of DEM application in search for novelty comminution devices is presented by Nordell and Potapov [20], where under a novel comminution machine concept, the Conjugate Anvil-Hammer Mill, DEM simulations enable performance comparisons against current equipment in the industry. DEM applications address the study of granular and discontinuous materials by analyzing particle flow, packing, transport, and mixing. DEM not only encountered applications in mining but also in other industries, such as pharmaceutical and food. Just to mention a few examples in the vast literature, it is observed in applications like design of eccentric feed hoppers for tablet presses [21], simulations of drying of wood chips in a baffled laboratory rotary dryer [22], optimization of a circularly vibrating screen [23], new design of SAG mills end liners [24], investigation of mill rotor shape in centrifugal bead mill [25], and design and optimization of a planetary gear [26].

To carry out a more realistic analysis inside crusher devices is necessary simultaneous simulation of flow particles and breakage, as well as the use of non-spherical particle shapes [27]. Analysis with non-spherical particles allows capturing a wider range of geometric characteristics of crushing devices and consequently determining if the analyzed geometries can crush particles more efficiently, as shown in the case of ellipsoidal particles [28]. According to the approach taken to model the generation of the progeny particles after collision events, different approaches to breakage modeling were presented and analyzed in the literature [29]. Where models based on the particle replacement approach, such as the model proposed by Cleary [30] or the one presented by Tavares et al. [31], allow a better application for crusher device simulations.

Taking advantage of the entire potential of DEM analysis, besides the current development of DEM simulations that are increasingly realistic, this paper aims to present the methodology used in the search for a novel comminution device. The presented methodology addresses the entire design process, from the solution concept generation to the concretization of the optimized final prototype for a comminution device. The optimization of characterized parameters is achieved through the application of computational methods FEM-DEM. As the DEM simulations are the principal tool in testing and choosing the proposal of the new comminution device, commercial software Rocky DEM is used to perform the simulations.

The paper is structured as follows: Section 1 outlines the approach to discrete element method objectives and their potential applications in the design of crushers. Section 2 examines in depth the steps that constitute the proposed methodology, accompanied by its application in the development of an innovative device design. In Section 3 general results are discussed. Finally, in Section 4 conclusions are given.

2. Materials and Methods

The final prototype layout of the new comminution equipment is depicted in Fig. 1. The process flowchart used to develop the novelty comminution machine is depicted in Fig. 2. The methodology is divided into four stages:

- Stage 1, Concept generation.
- Stage 2, Shapes generation.
- Stage 3, Calculation and selection of the machine elements.
- Stage 4, Structural Analysis.

Table 1. Listed needs - Raw data.

• High capacity.	• Easy to change liner.
• Low operative cost.	• Removable lining.
• Low energy consumption.	• Reliability.
• Low components wear ratio.	• Low risks of injuring the operator.
• Wear resistant lining.	• Low risks of damaging the equipment.
• High efficiency.	• Low risks of bad operability.
• Efficient use of energy.	• Shut down in case of overload.
• Easy maintenance.	

2.1. Concept generation

The concept generation was structured based on the guidelines presented by Ulrich and Eppinger [32]. Four steps are established to achieve the process. The first step is the identification of needs, the second step is the establishment of the specifications, the third step is the generation of the concepts of solution, and finally, the fourth step is the choice of the best concept.

In the first step, the process consists of the identification of the principal customer necessities. Needs are collected, then are hierarchized and ranked by importance. The collection of the needs follows criteria such as maintenance and practicality. The identified needs that are tagged as *raw data* are shown in Table 1.

The second step, the establishment of specifications, is achieved by translating the ranked raw data into punctual requirements for new comminution devices. The third step, the generation of the solution concepts, is addressed following three sub-steps. The first sub-step is the clarification of the process. According to Ulrich and Eppinger [32] the black box, which represents the overall function of the novel device, should be decomposed into sub-functions or sub-problems. The black box subfunctions are represented by material, energy, and signal operating flows, as shown in Fig. 3.

The second sub-step is an external search for solutions. As the aim of the present paper is to design a new comminution machine, the decompound process is key in the analysis of the sub-functions, especially in how to apply converted energy to the mineral. Several concepts of solution that could solve the subproblems were proposed, such as decompound by compression, decompound by ore-ore impact, decompound by ore-surface impact, decompound by ore-surface abrasion, decompound by ore-ore abrasion, decompound by P wave [33], decompound by leaching and decompound by bioleaching. The third sub-step is the systematic exploration of potential solutions. It is accomplished by the combination of concepts of solutions that have been proposed to solve the subfunctions. As a result, several solutions for the comminution device are obtained from combinations, principal solutions are listed below:

A. Mill with internal rotor: This conceptual solution uses an internal rotor placed into a mill rotating with an angular velocity, higher than the critical required. the model aims to promote collisions between particles placed in the internal wall mill with particles that are thrown by the internal rotor (Fig. 4(a)).
B. Impact crusher conducted by a sprinkler: This machine aims to instigate the ore-ore impact break mechanism through two feeding inputs. One input lets one group of particles enter through the equipment periphery, while the second input lets the other group of particles enter through an internal rotor which impulse them to impact the first group of particles (Fig. 4(b)).
C. Impact spoon: This equipment uses a rotor whose blades present a cavity where groups of particles are propelled against input particles that fall by gravity (Fig. 4(c)).
D. Double rotor impactor: This proposal uses two rotors to make the particles impact each other producing breakage (Fig. 4(d)). As a result, this equipment presents the particle breakage system based on decompound by ore-ore impact.

Finally, in the last step, the generated solutions were scored in a selection matrix, the concepts were weighted regarding productivity, energy consumption, primary needs satisfaction, innovation, safeness, manufacture costs, technological complexity, delivery term, availability, structure materials, ease of assembly, maintenance, operability, and environmental impact. As a result, the concept of solution D “Double rotor impactor” is chosen.

2.2. Shapes generation

The generation of shapes and dimensions for the device is addressed in three stages, that follow the subfunctions of the concept of solution pattern.

2.2.1. *Shape of the surrounding geometry of the rotors*

This stage involves the structure that interacts with the rotors. The final geometry aims to receive, store, direct the minerals toward proper contact with the rotors and finally, direct the products to the outlet. Figure 5 shows the three prototypes proposed according to the feed pattern. The geometry shown in Fig. 5(a) aims for a transversal inlet that lets particles be positioned just before the contact with the rotors. Geometry presented in Fig. 5(b) aims to impulse the particles toward a surface or other particles, to achieve this, the particles are conducted toward a tangential position to the contact with the rotors. Finally, in Fig. 5(c) the aim is that the particles fall toward contact with the rotors, thus a single entry in the upper middle zone that allows the feed to be bifurcated is proposed. To carry out DEM simulations, an initial trial shape of the rotor is established.

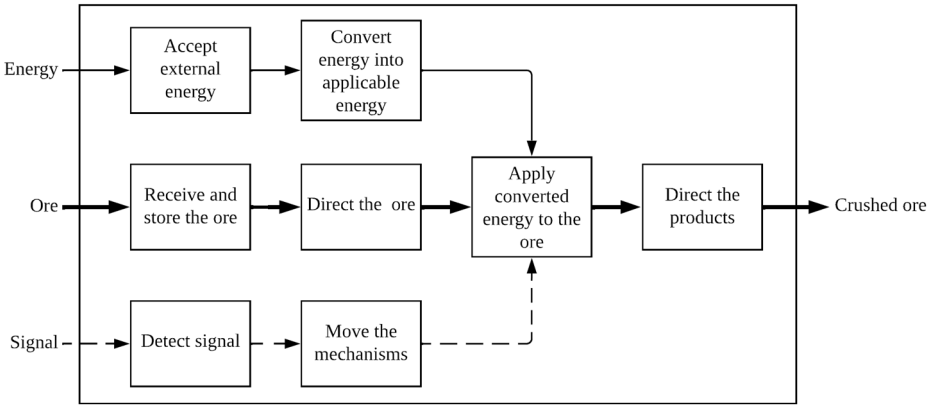

Fig. 3. Functional diagram of a novelty comminution machine from a functional decomposition. It shows the subfunctions obtained from the refinement of the black box.

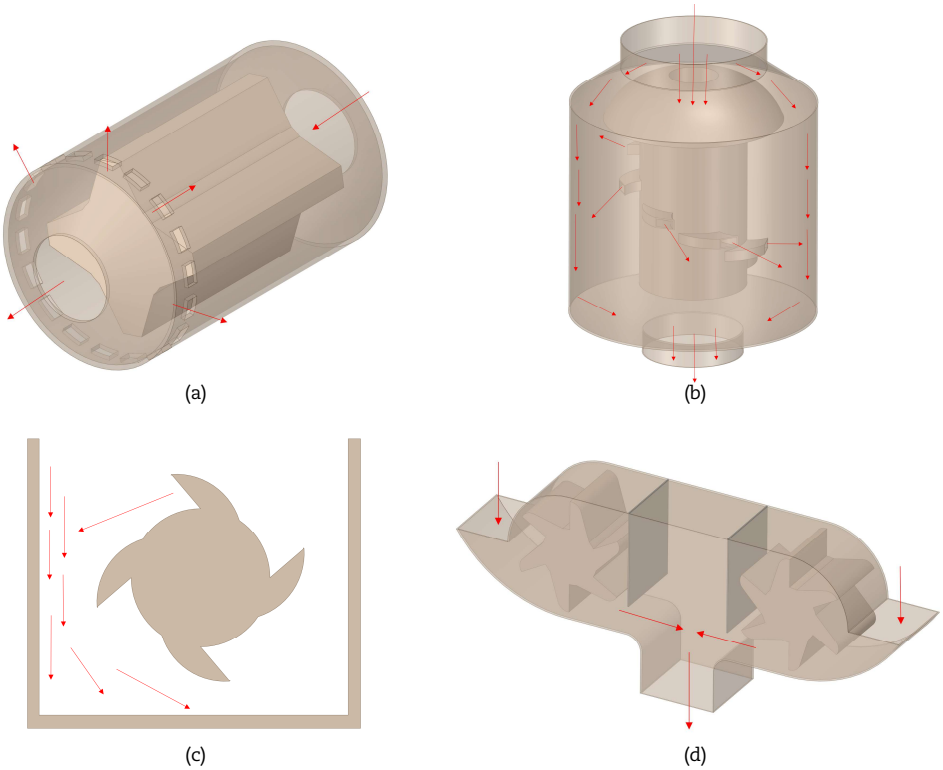

Fig. 4. Comminution machines design proposals. (a) Mill with internal rotor. (b) Impact crusher conducted by a sprinkler. (c) Impact spoon. (d) Double rotor impactor. Red arrows represent the mineral flow through the machines.

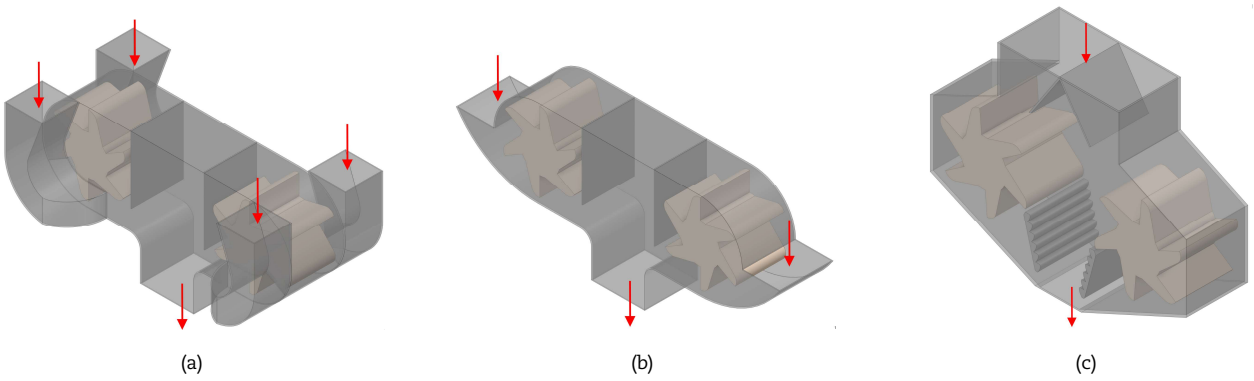

Fig. 5. Prototypes of the machine based on feed pattern. (a) Transversal feed. (b) Lateral feed. (c) Top feed. Red arrows indicate inlets and outlets of minerals. It is possible to observe how are distributed the inlets.

2.2.1.1. *DEM Simulations*

To decrease the computational cost of the DEM simulations, the so-called Energy Spectra tool was performed instead of a complete breakage analysis. Energy spectra enables the collection of collision statistics per collision type, values for contacts inter particles and particles with each internal component of the prototypes (rotors, inlet surfaces, internal plates, outlet surfaces, etc.) are stored and then analyzed. The parameters used in the configuration are summarized in Table 2. For each prototype, three different rotor speeds (700, 1200, and 1800 rpm) are tested.

Table 2. Parameters used in DEM simulations.

Contact model			
Normal force	Hysteretic Linear Spring		
Tangential force	Linear Spring Coulomb Limit		
Mechanical properties			
Ore	Density	2500	kg/m^3
	Young modulus	1.00E+08	N/m^2
	Poisson's ratio	0.3	-
Surfaces	Density	7850	kg/m^3
	Young modulus	1.00E+11	N/m^2
	Poisson's ratio	0.3	-
Rigid ball particle parameters			
Diameter		0.02	m
Number of particles		1328	-
Feed		10	t/h

The analysis of the results is based on the comparison of the cumulated specific power of the total number of particle collisions. However, since the aim of the structure is to promote an efficient interaction between particles and rotors, the analysis is focused on the power generated for the couple particle-rotor. The results of the total cumulated power of the couple are shown in Fig. 6. There is a notable difference in the performance of the prototypes in support of the top feed. Additionally, the results show the highest cumulated specific power at 1800 rpm, which is a representative speed. It is possible to infer that the top feed allows for better contact between particles and the rotor compared to the other proposals, consequently, the prototype with the top feed is selected.

2.2.2. *Shape of the rotors*

In this section, six prototypes of the impact rotors were proposed, as shown in Fig. 7. For the six shapes presented, the concept and form of the rotor proposed in solution concept C (Fig. 4(c)) shown earlier has been taken as the baseline reference. The generation of the six alternatives shown in Figure 7 is the result of an intensive investigation, innovation and evaluation with DEM of alternatives geometries to the initially proposed, also some insights from the industry was considered. The following analysis aims to identify which of the rotors have the best performance promoting breakage.

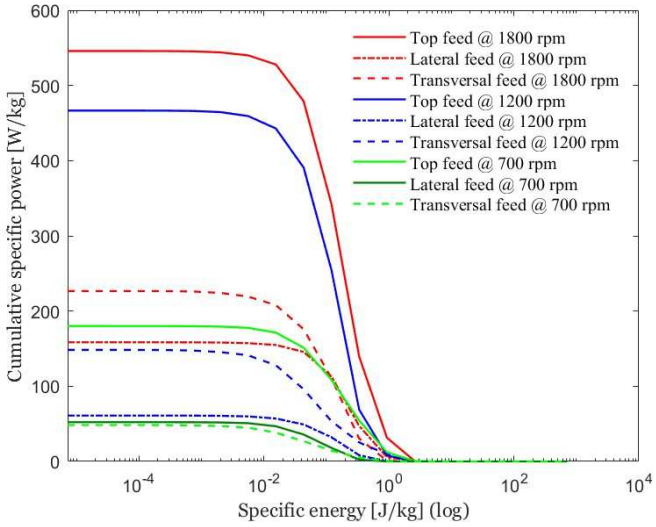

Fig. 6. Energy spectra curves of surrounding structure prototypes.

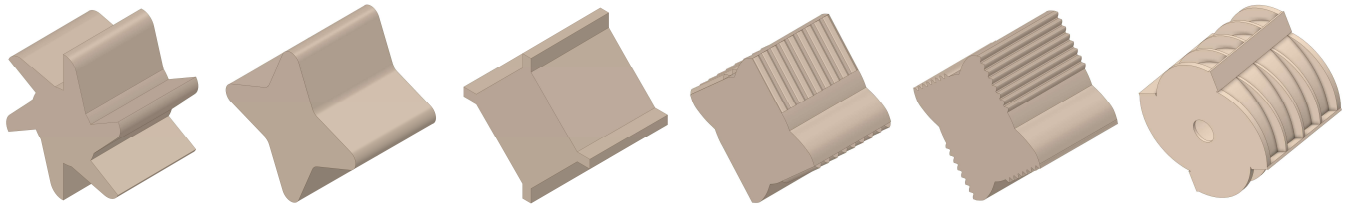

Fig. 7. Proposed rotor prototypes. (a) Rotor A. (b) Rotor B. (c) Rotor C. (d) Rotor D. (e) Rotor E. (f) Rotor F.

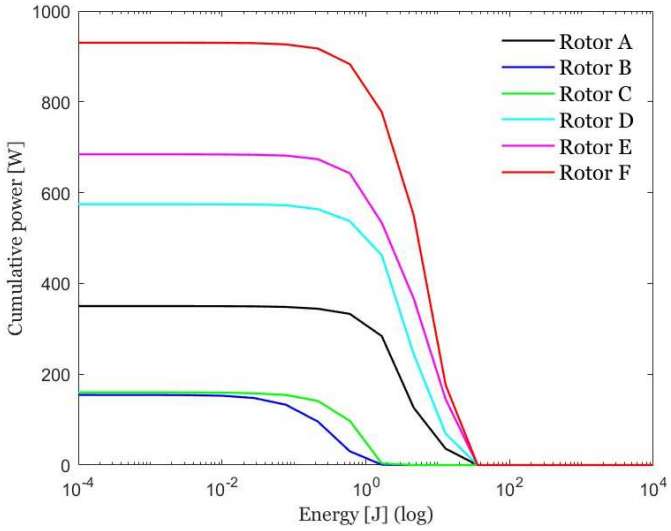

Fig. 8. Energy spectra curves of rotor prototypes.

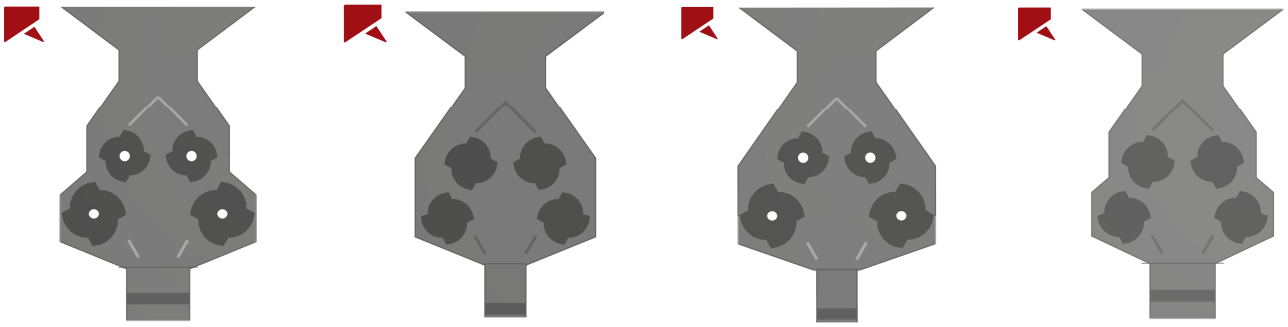

Fig. 9. Final prototypes. (a) Prototype A: Structure A with two different pairs of rotors. (b) Prototype B: Structure B with four equal rotors. (c) Prototype C: Structure B with two different pairs of rotors. (d) Prototype D: Structure A with four equal rotors.

2.2.2.1. *DEM Simulations*

To achieve rotor prototype performance comparisons, energy spectra of cumulated power in interactions between particles and rotor are analyzed as well. The tests are carried out using the surrounding rotor's shape selected previously. Simulations were configured for each rotor prototype rotating at 1800 rpm. Additional parameters were input according to the information in Table 2. Simulation results are presented in Fig. 8, where the cumulated power curve of prototype F has reached the highest values in comparison to the others, therefore, prototype F is selected.

2.2.3. *Shape of the final prototype*

Once the structure and rotor shapes have been defined, final dimensions, such as the separation between rotor axes or the drop height of the particles need to be settled. Figure 9 shows the four final prototypes proposed for the analysis. Two final structure shapes are combined with two different arrangements of four rotors. The structure shapes present just slight modifications concerning the shape selected in the previous section. The new structure shapes are tagged as Structure A and B. Figures 9(a) and 9(d) show Structure A in combination with two pairs of rotors of different sizes, in the same way, Figs. 9(b) and 9(c) use Structure B. The aim of the process is that the pair of rotors placed on the top would generate the greatest number of broken particles. On the other hand, the pair on the bottom should achieve the rupture of missed particles and complete the rupture of big-size fragments resulting from the initial collisions to obtain a proper product particle size.

2.2.3.1. *DEM simulations*

Several DEM simulations were carried out including the breakage option using the so-called Tavares Model [34]. Limestone is a representative material chosen to model the final prototypes. Tavares breakage input parameters were collected from Andre et al. [34], and presented in Table 3. Table 4 presents other required parameters.

In the first simulation stage, particle movement and values of size reduction, presented in Fig. 10, are analyzed. It can be noted that, in general, the particle sizes range from 20 mm to about 6 or 7 mm. So, at first instance, there is not a notable difference between the prototype's performance. However, Structure A promotes less accumulation of particles close to the walls, therefore, less pressure is applied over the structure. Simulations show that the particles are broken in the first collision, so the difference in the structure shapes does not disturb breakage behavior. Results for more exhaustive simulations carried out in the second stage are shown in Fig. 11. In this stage, the analysis is focused on the particle size of products. Comparisons show a slightly superior performance of the final prototype A, composed of Structure A with the arrangement of different rotor sizes. Finally, based on previous results, the prototype A is chosen as the final model of the device.

Finally, the last simulation of the selected final prototype was performed to establish the reduction ratio. The simulation is presented in Fig. 12, analysis shows that the prototype reduced the particle size from 20 mm to about 1.00862 mm, which means a ratio of 1:20. Results can be considered satisfactory, taking into account that machines such as jaw crushers, can reach ratios of 1:7 [35].

Table 3. Parameters of the Tavares breakage model.

Parameter	Sub-parameter	Numeric value
Limestone – Structure interaction	Static friction coefficient	0.3
	Dynamic friction coefficient	0.3
	Tangential modulus ratio	1
	Restitution coefficient	0.3
Limestone – Limestone interaction	Static friction coefficient	0.6
	Dynamic friction coefficient	0.6
	Tangential modulus ratio	1
	Restitution coefficient	0.5
Particle shape data (polyhedral)	Vertical ratio	1
	Horizontal ratio	1
	Number of corners	50
	Super-quadratic grade	2
Particle breakage parameters (Tavares model)	σ^2	0.642
	e_{max} / e_{50}	4
	e_{min}	1 [J/kg]
	e_{∞}	7 [J/kg]
	d_0	0.1 [m]
	ϕ	0.8
	γ	5.4
	A	53.3
	b'	0.033

Table 4. Parameters used in DEM breakage simulations.

Contact model			
Normal force		Hysteretic Linear Spring	
Tangential force		Linear Spring Coulomb Limit	
Mechanic parameters			
Limestone	Density	2710	kg/m^3
	Young modulus	5.00E+08	N/m^2
	Poisson's ratio	0.3	-
Surfaces	Density	7850	kg/m^3
	Young modulus	1.00E+11	N/m^2
	Poisson's ratio	0.3	-
Polyhedric particle parameters			
Equivalent diameter		0.06	m
Number of particles		4	-
Feed		10	t/h
Breakage parameters			
Model		Tavares breakage	
Particle size distribution	Model	Gaudin-Schumann	-
	Minimum size	0.001	m

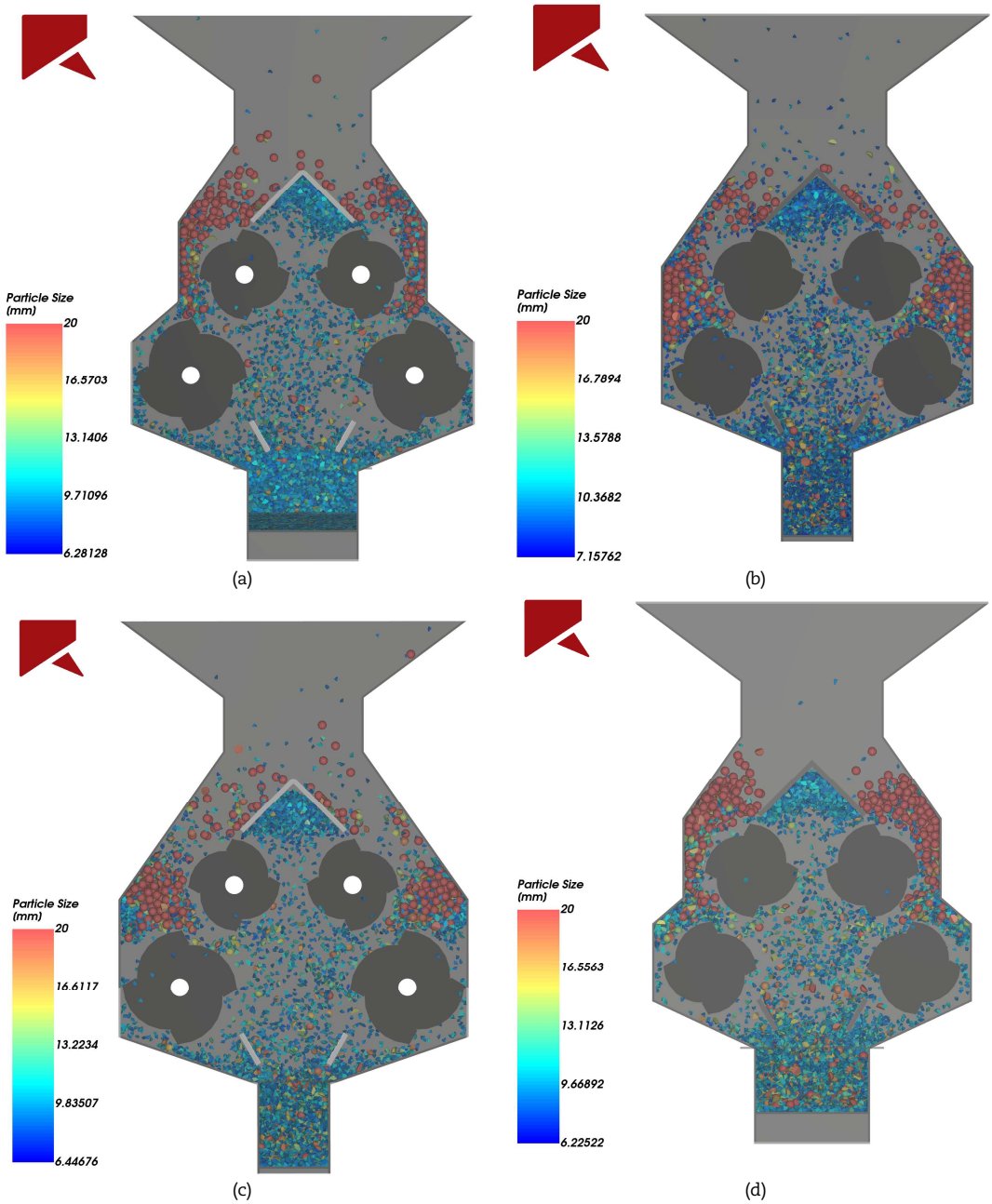

Fig. 10. Particle breakdown results of final prototypes. (a) Prototype A. (b) Prototype B. (c) Prototype C. (d) Prototype D. The flow of particles and broken fragments within the prototypes are shown. The crucial role of the plates in guiding the products can be noted.

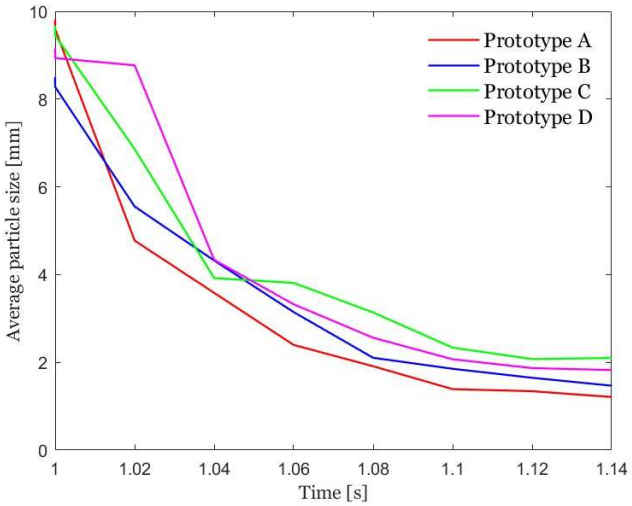

Fig. 11. Product particle size for final prototypes. Prototype A in red curve color, which combines Structure A with different pairs of rotors, reaches the minimal values of the average product particle curve at the end of the simulation.

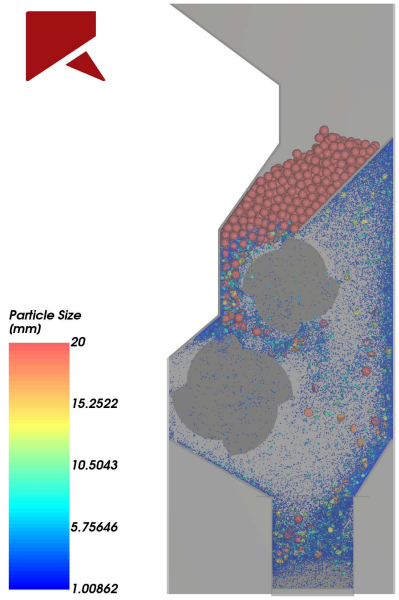

Fig. 12. Particle size reduction in a final prototype selected.

2.3. Calculation and selection of the machine elements

2.3.1. *Power calculation*

In order to calculate the required power rating, it becomes necessary to identify the loads and total momentum applied to the rotors. Once these variables are known, the following equation is applied:

$$P = wMf_s \tag{1}$$

where P stands for power consumption, w is the angular velocity, M is the resultant momentum at the rotors, and f_s is the factor of safety corresponding to the operational conditions. The resultant moment M is obtained from the DEM analysis by extracting the reactant moment calculated in the rotor shaft. Also, a standard safety factor f_s of 2 is considered in order to cover mechanism inaccuracies. The corresponding moment values M for the superior and inferior rotors are 5.4407 N.mm and 2.4185 N.mm, resulting in power consumptions of about 2.05 kW and 0.92 kW, respectively. Therefore, motors of 2.2 kW (3 hp) and 1.5 kW (2 hp) are selected.

2.3.2. *Drive system calculation*

The chosen transmission system for this machine relies on belt drives due to the high angular velocities in the rotors. The calculation follows the procedure outlined by Mott [36]. Figure 13 illustrates the configuration of the belt drive, with Figs. 13(a) and 13(b) depicting the superior and inferior rotors, respectively.

The required design power is determined by multiplying the power rating of the motors by the required service factor. The service factor *Sf*, based on the driven load and considering the AC motor normal torque, operation for a maximum of 15 hours per day, and moderate shock loading, as specified by Mott [36], is found to be 1.3. Consequently, the design power for both types of rotors is calculated as 2.9 kW and 1.95 kW, respectively.

In terms of belt parameters, a 3V belt cross-section is recommended due to the speed of the selected input rotors, which corresponds to 1800 rpm. The machine is designed to utilize sheaves with equal pitch diameters, resulting in nominal speed ratios of 1. With the recommended belt speed of 20 m/s, the calculation of the sheave diameters yields approximately 215 mm. Verification

is conducted with a trial diameter of 200 mm being selected. Accordingly, a pitch diameter of 200 mm is selected for the sheaves. Furthermore, the rated power per belt is determined to be 7.45 kW for both the superior and inferior arrangements.

According to Mott procedures [36], the center distances *CD* and belt length values for the superior rotor result in 748 mm and 2159 mm, respectively, and for the inferior rotor result in 634 mm and 1905 mm, respectively.

Finally, in order to obtain corrected power ratings, the wrap correction factor C_θ and the belt length correction factor C_L were selected. Those values were estimated taking into account information described in Chapter 7 of Mott [36]. For belt lengths of 2159 mm and 1905 mm, and an angle of contact of 180°, the selected values are C_θ equal to 1 for both superior and inferior rotors, C_L equal to 1.06 for superior rotor and C_L equal to 1.04 for inferior rotor. The corrected rated power for each rotor is calculated by multiplying C_θ by C_L by the value of power per belt previously calculated. Therefore, the corrected rated power for the superior and inferior rotors are 7.9 kW and 7.75 kW, respectively. Dividing the design power over the corrected power rating per belt, the minimum number of belts results in 0.37 and 0.25, which means that in both cases, at least 1 belt is required for each rotor.

2.3.3. *Shaft calculation*

In the previous procedure, all motor-shaft rotors resulted in the same sheave size. However, as each pair of rotors presents different loads and torques, two shaft models are calculated following the same calculation process detailed below. The shaft calculation process starts by extracting the loads and torques at the center of both different rotors shafts obtained from the DEM analysis. According to Mott [36], tensions at sheaves must fulfill the following equation:

$$\frac{T_2}{T_1} = 5 \tag{2}$$

where T_2 is the tight side tension and T_1 is the slack side tension.

Figure 14 depicts the general schematic of the forces applied to each shaft. Both shafts have the same geometry and arrangement of components; however, the forces have different magnitudes. It should be noted that the values of the loads are obtained from DEM analysis. In the figure, R_1 and R_2 represent the reactions of the bearings on the shaft. Each rotor is coupled to each shaft by two keyways, and the corresponding loads are represented by the forces F_{rotor1} and F_{rotor2}. The weight of each rotor is represented by two loads applied at the contact points with the keyways, represented by W_{rotor1} and W_{rotor2}. Last but not least, the weight of the pulley W_{pulley} and the load due to the tension F_p are considered. The loads on the shaft are analyzed, and force diagrams for shear forces and bending moments accompany the calculation. The torsional moment at each point of each shaft is also calculated.

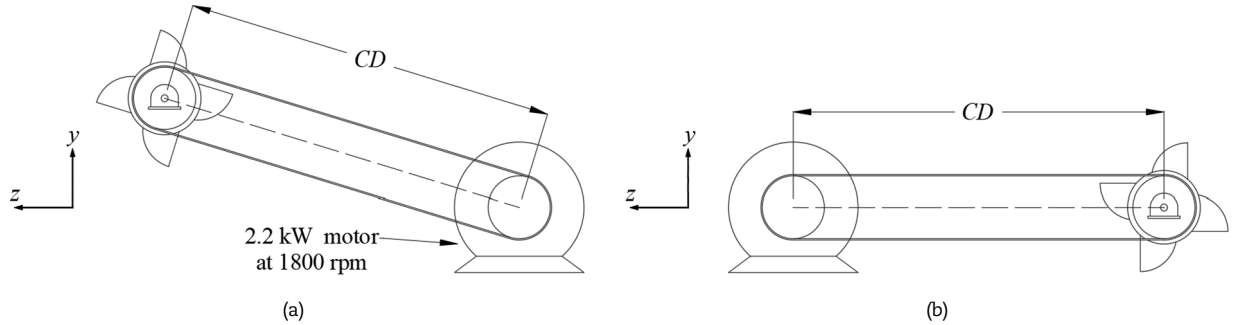

Fig. 13. Belt drive configuration for the superior, (a) and inferior (b) rotors.

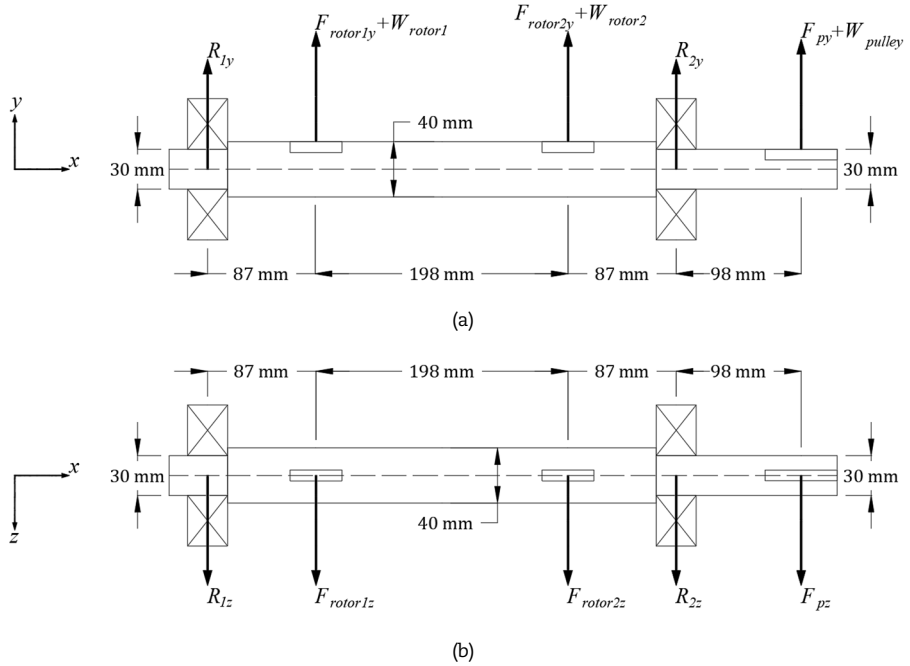

Fig. 14. Loads applied on the shaft (a) loads applied in the plane yx, (b) loads applied in the plane zx.

After the identification of the loads and moments acting at the shafts, the next step is to calculate the shaft diameters. It starts by obtaining a pre-calculated diameter [38] which is then verified to fulfill some criteria:

$$d_{pre} = \sqrt[3]{\frac{16T}{\pi\tau_{tPUL}}FS} \tag{3}$$

where T is the torsional moment at the evaluated zone, τ_{tPUL} is the pulsating shear stress of the material shaft, and FS is the recommended uncertainty factor, whose value depends on whether it is subjected to torsional and bending moments or only torsional moments.

The calculations focus on the most critical zone of the shaft, where the highest bending moments are applied. According Fig. 14, this zone corresponds to the position where the force R_2 is applied, with the correspond bending moment values of 19315.078 N.mm and 12545.746 N.mm for the superior and inferior shaft, respectively. Additionally, the maximum torsional moments for the superior and inferior shafts at that position are 11867.832 N.mm and 14918.088 N.mm, respectively. Considering an uncertainty factor FS of 15, recommended factor for rough calculation of torsional stress [38], additionally considering fatigue strength under pulsating load τ_{tPUL} equals to 170 MPa for St37-2 steel [40]. The precalculated diameter for the superior and inferior shaft is 17.471 mm and 18.856 mm, respectively. However, a diameter of 30 mm is used for both shafts, taking into account the keyways dimensions.

To ascertain the adequacy of the precalculated diameter, the fatigue criteria are applied. The following safety factor FS_{fat} must be at least 1.5 [38], the following equations are used:

$$FS_{fat} = \frac{\sigma_{fAL}}{\sigma_v} \tag{4}$$

$$\sigma_v = \sqrt{(\sigma'_f)^2 + 3(\alpha_0\tau'_t)^2} \tag{5}$$

$$\alpha_0 = \frac{\sigma_{fAL}}{1.73\tau_{tPUL}} \tag{6}$$

$$\sigma'_f = \frac{\beta_f}{C_s C_t C_c C_{temp}}\sigma_f \tag{7}$$

$$\tau'_t = \frac{\beta_t}{C_s C_t C_c C_{temp}}\tau_t \tag{8}$$

$$\beta_f = 1 + n_k(\alpha_f - 1) \tag{9}$$

$$\beta_t = 1 + n_k(\alpha_t - 1) \tag{10}$$

$$\sigma_f = \frac{32M_f}{\pi d^3} \tag{11}$$

$$\tau_t = \frac{16M_t}{\pi d^3} \tag{12}$$

where σ_{fAL} is the alternating normal stress, σ_v is the equivalent stress, α_0 is the effort ratio according to C. Bach, C_s is the coefficient for surface finish, C_t is the coefficient for diameter, C_c is the coefficient for reliability, C_{temp} is the coefficient for temperature, β_f is the concentration factor of bending effective stresses, β_t is the concentration factor of torsional effective stresses, n_k is the notch sensitivity factor according to Thum, α_f is the shape factors of notched round bar under bending stress, α_t is the shape factors of notched round bar under torsional stress, τ_{tPUL} is the pulsating shear stress of the material shaft, M_f is the bending moment at the evaluated zone, M_t is the torsional moment at the evaluated zone and d is the shaft diameter.

Table 5. Values of fatigue criteria parameters.

	Superior Shaft	Inferior Shaft
σ_{fAL}	200 [MPa]	200 [MPa]
τ_{tPUL}	170 [MPa]	170 [MPa]
σ_v	21.109 [N.mm]	15.041 [N.mm]
α_0	0.679	0.679
C_s	0.941	0.941
C_t	0.862	0.862
C_c	0.814	0.814
C_{temp}	1	1
β_f	1.84	1.84
β_t	1.44	1.44
n_k	0.4	0.4
α_f	3.1	3.1
α_t	2.1	2.1
M_f	19315.078 [N.mm]	12545.746 [N.mm]
M_t	11867.832 [N.mm]	14918.088 [N.mm]
r	0.6 [mm]	0.6 [mm]
d	30 [mm]	30 [mm]

Table 5 summarizes the values and results of equations (4) to (12). The coefficients C_s, C_t, C_c, and C_{temp} are obtained from Shigley's chapter 6 [37]. The values of the coefficients n_k, α_f and α_t are obtained from Steinhilper & Röper, chapter 3 [39]. Equations (5) and (6) are settled according to Köhler, section of Development of the calculation procedure for shafts and axles [38]. Finally, values of σ_{fAL} and τ_{tPUL} obtained from [40]. As a result, taking into account the geometric dimensions of the shaft, the diameter d and the notch radius r, the safety factor FS_{fat} for the upper and lower shafts is 9.475 and 13.297, respectively.

2.4. Structural analysis

2.4.1. *FEM analysis*

Once favorable safety factor values for both the lower and upper shafts have been achieved, the next step is to examine the potential occurrence of resonance effects. This involves comparing the operational rotating speed with the rotating speed corresponding to the natural frequency. Utilizing rotodynamic FEM analysis, the first four modes of both shafts with their rotors and pulleys are obtained, depicted in Figs. 15 and 16. According to Köhler [38] and Steinhilper & Röper [40], the ratio of operational rotating speed to the rotating speed corresponding to the natural frequency should be less than 0.8 or greater than 1.15 to ensure sufficient distance from the resonance zone. Based on the DEM analysis, the operational rotating speed of the shaft is determined to be 1800 rpm or 188.496 rad/s. Additionally, the lowest natural frequency values for both the upper and lower shafts are found to be 295.55 Hz or 1857 rad/s, and 299.4 Hz or 1881.19 rad/s, respectively. Consequently, the rotating speed ratios for both shafts are approximately 0.1, indicating operation under sub-critical conditions.

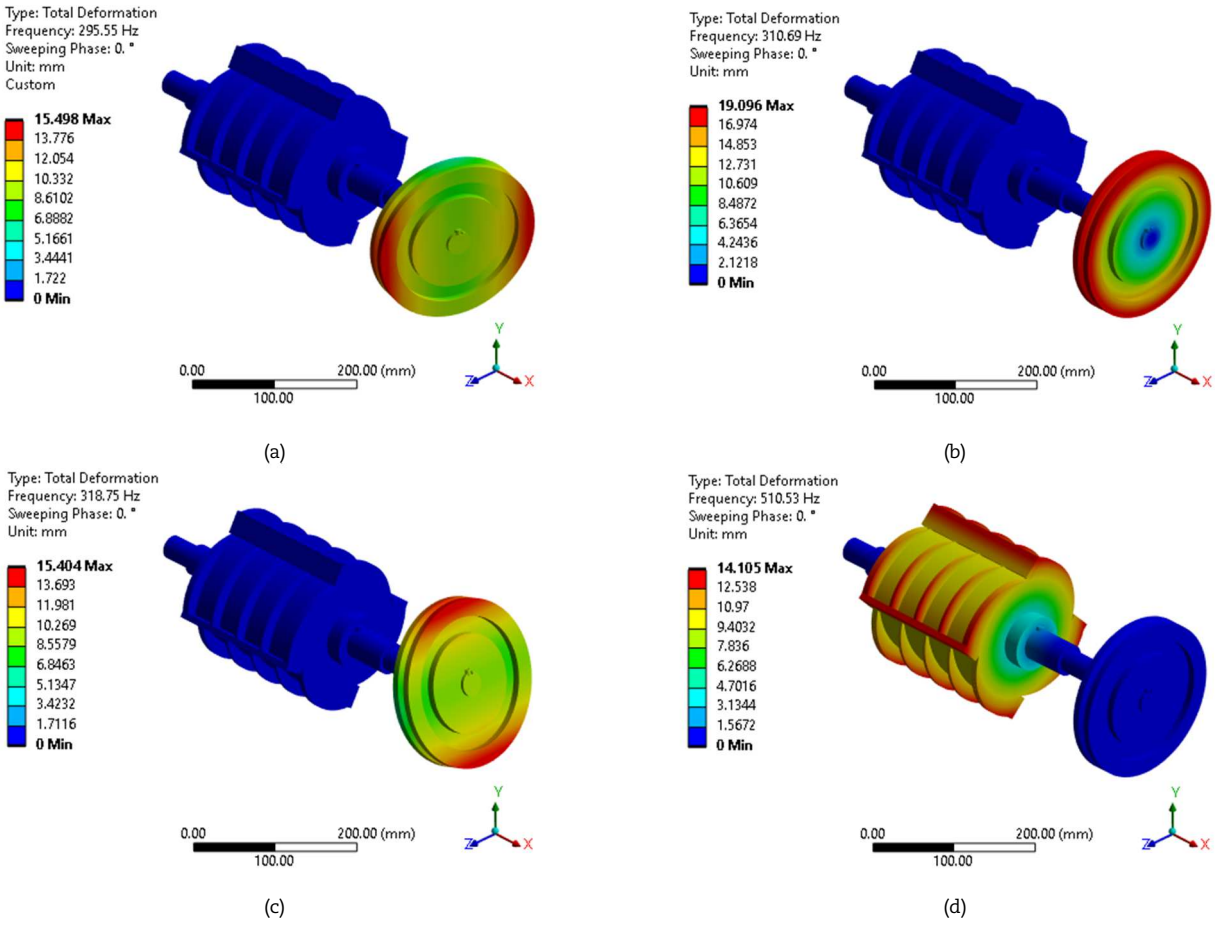

Fig. 15. Modal analysis of the superior rotor. (a) First mode. (b) Second mode. (c) Third mode. (d) Fourth mode.

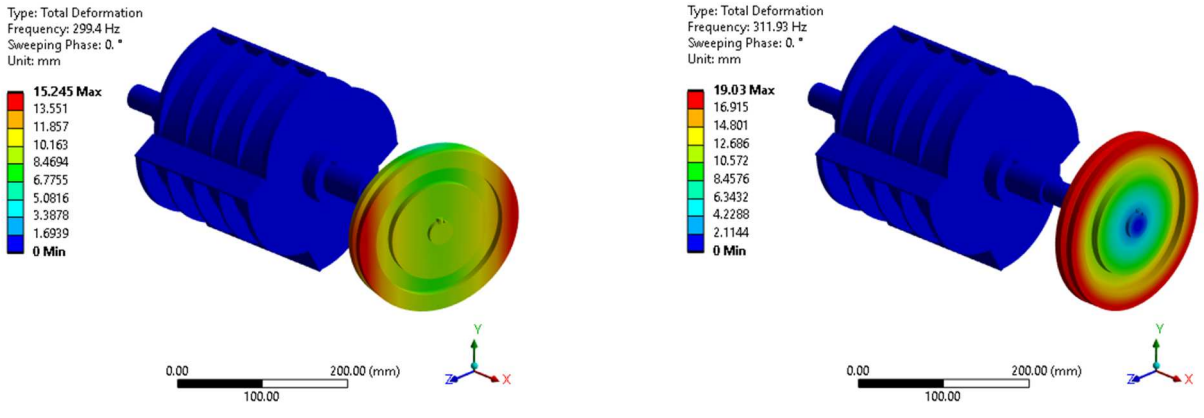

Fig. 16. Modal analysis of the inferior rotor. (a) First mode. (b) Second mode. (c) Third mode. (d) Fourth mode.

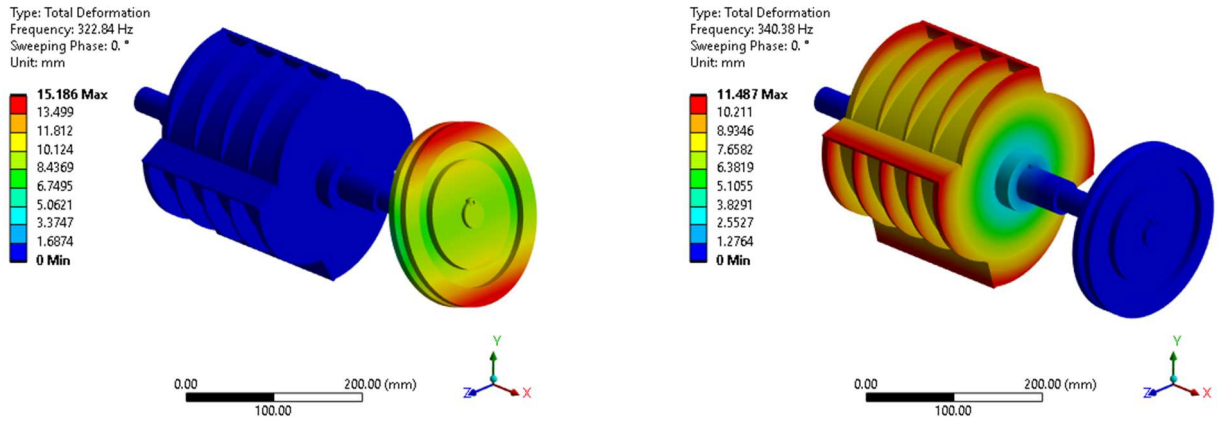

(c) (d)

Fig. 16. Continued.

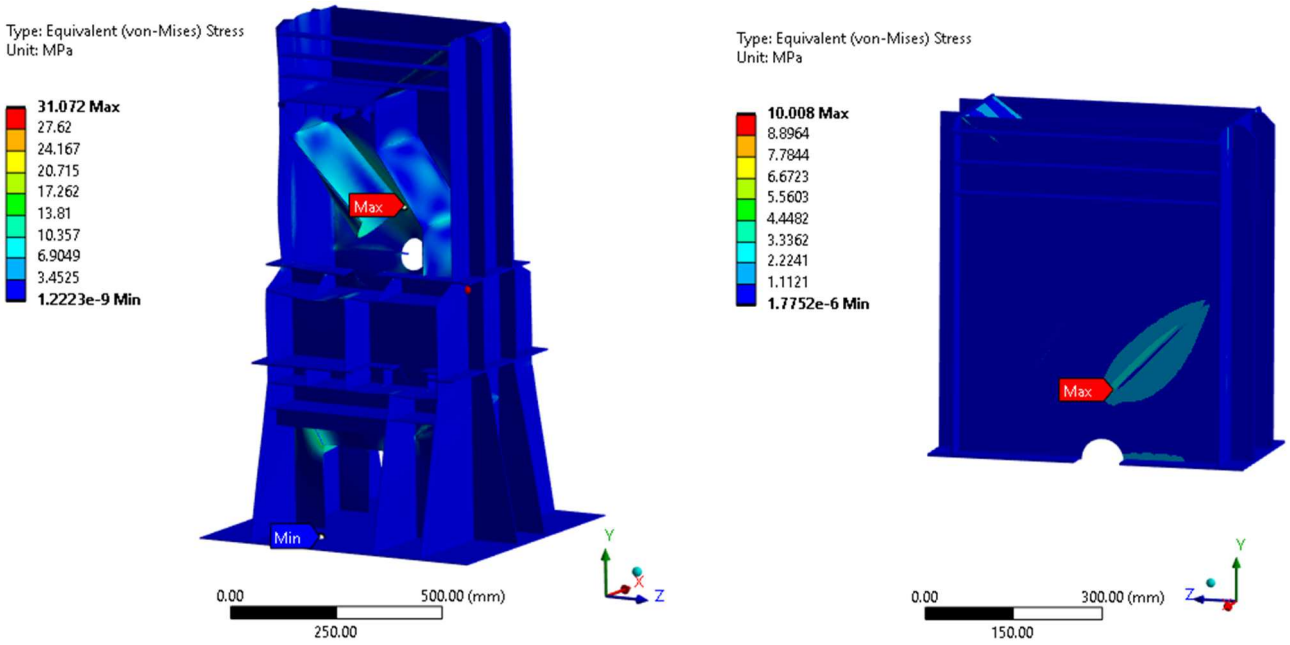

(a) (b)

Fig. 17. Von-Mises equivalent stress in a Double rotor impactor machine. (a) Final prototype results. (b) Reinforced model with simplified geometry.

Concurrently, the structural analysis of the machine is conducted using the finite element method (FEM) and mechanical loads derived from the DEM analysis. A mesh convergence study was conducted, focusing on the equivalent Von Mises stress. Based on an initial simulation, a quadratic adaptive mesh refinement was applied, increasing the configuration from 634,580 nodes and 193,524 elements to 1,309,382 nodes and 668,891 elements. This resulted in a final value of 31.072 MPa, representing a 5.2% variation from the initially obtained equivalent stress. Figure 17(a) shows the critical point where the maximum equivalent stress occurs, notably at the top of the structure. For comparison purposes, a subsequent analysis of this section was performed after adding reinforcements to the critical section. Similarly, a convergence analysis was carried out, refining the mesh from an initial configuration of 242,817 nodes and 102,532 elements to 2,051,197 nodes and 1,306,725 elements. The final quality of the tetrahedral mesh corresponds to a torsion metric value of 0.35. The final equivalent stress for the modified geometry is 10.008 MPa (Fig. 17(b)). However, for the safety factor calculation, the equivalent stress obtained in the original structure simulation is used. Considering the yield stress of 250 MPa for 2 mm thick ASTM A36 steel plates, a safety factor of approximately 8.05 has been determined for the structure. Since this safety factor for this machine in the mining industry is high, it appears that the slight variation demonstrated in stress calculations due to mesh refinement is not detrimental. Additionally, structural stability is assessed through modal analysis, with results depicted in Fig. 18. The analysis indicates that the lowest frequency value among the first four modes is 102.75 Hz. Given a motor speed of 1800 rpm and a frequency value of 29,990 Hz, the established working conditions do not reach the minimum natural frequency, ensuring structural stability.

Furthermore, the structural design features lower trapezoidal profiles on the sides, enhancing minimizing the potential for resonance in the rolling movement of the structure, particularly evident in the first vibration mode. Resonance in the second and fourth vibration modes is also mitigated by the support of the lateral profiles. To further mitigate resonance in the second vibration mode, adjustments have been made to the front and rear profiles, and the plate thickness has been increased. Following the evaluation of proposed structure dimensions, component arrangement around the mining equipment is developed. As illustrated in Fig. 19, a small deposit is incorporated at the lower position of the structure to collect crushed particles. Additionally, electric motors are positioned in side spaces of the equipment to transmit power to the two axes via belts and pulleys.

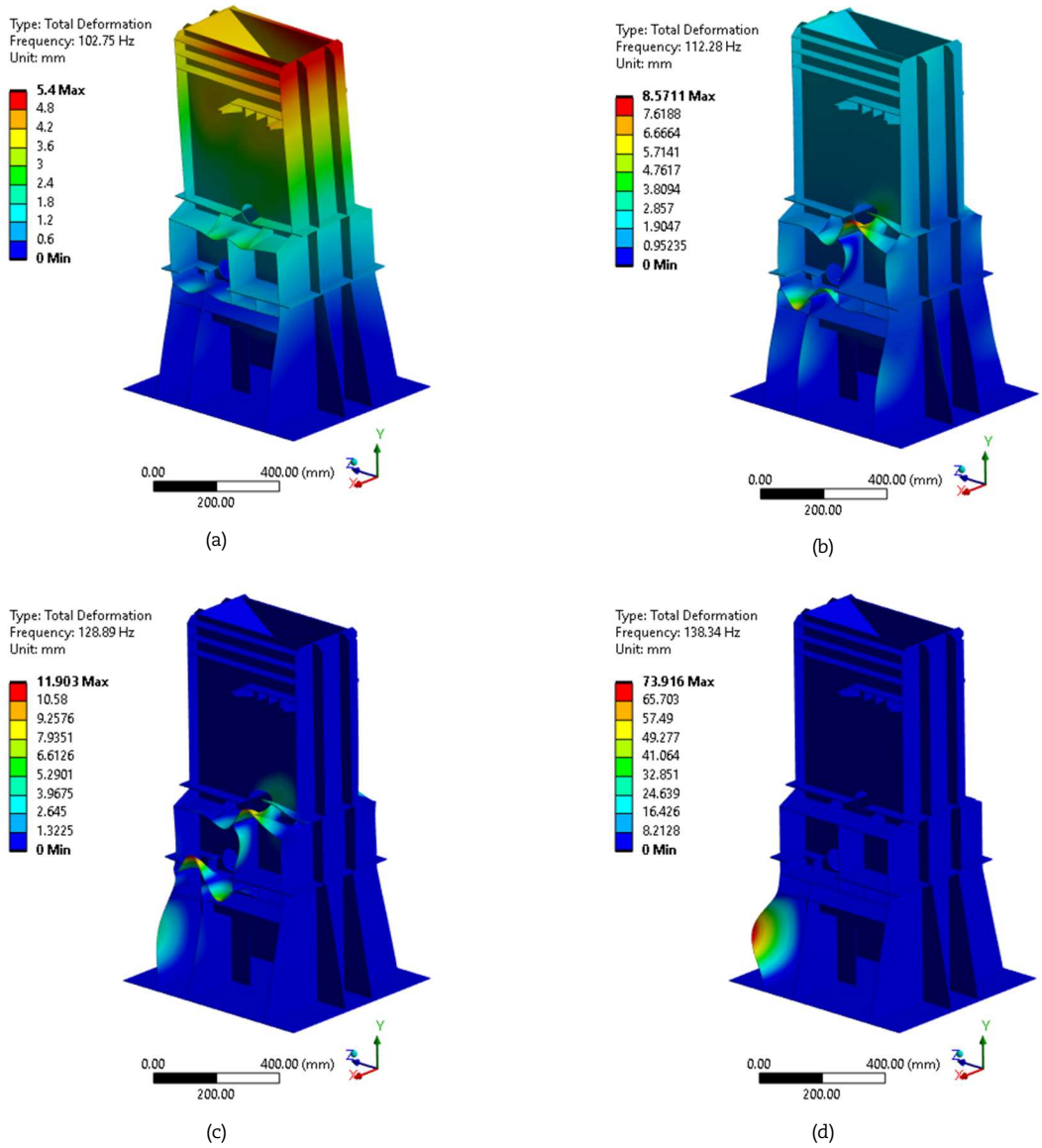

Fig. 18. Modal analysis of a Double rotor impactor final prototype. (a) First mode. (b) Second mode. (c) Third mode. (d) Fourth mode.

3. Discussion

Following the staged process outlined in Section 2, the final prototype is depicted in Fig.19. Additionally, Fig. 20 displays the constructed model. Besides its inherent function, the machine can be adapted to function as an experimental setup for breakage testing. In this setup, particles of arbitrary sizes can be dropped onto the machine from above to be impacted by one of the rotors. The resulting particle size and the energy generated by the rotor impact can then be measured and correlated to support the development of new breakage approaches. As a logical outcome of the simulation process, the presented design method offers the advantage of assessing and prioritizing various comminution design concepts, optimizing them to their fullest extent, and postponing the manufacturing of prototypes for effectiveness testing until the final stages. This approach effectively reduces costs associated with the design process.

Once more, as indicated in the literature, DEM simulations have demonstrated their potential as the primary tool for developing prototypes of comminution devices and establishing operational parameters. DEM enables designers to directly leverage their creativity. Thus, developing a robust breakage model is key to eventually eliminate the need for real experimentation. Progress in this area will achieve more closely mirror real-world conditions. The outcomes of this effort will result in substantial benefits for design processes, efficiency, and cost savings.

The contribution of this work lies in the presentation of the methodology, which combines techniques and procedures that could achieve innovative design. The elaboration of the design concept and the analysis of particle treatment processes rely on a set of tools, including analytical hierarchical criteria and the decomposition of complex problems described by Ulrich and Eppinger [32], to organize the best design solution concepts. Additionally, the use of DEM to achieve comparisons, serving as the main tool, based on particle energy spectra to evaluate the efficiency of each solution concept in particle treatment with low computational cost. Furthermore, the complementary application of the Tavares breakage model analyzes particle fragmentation for all variations of the prototypes. The integration and organization of these processes contribute to a comminution machine design method capable of creating, ranking, evaluating, and calculating new comminution machine concepts.

To address the reduction of computational costs, within the DEM approach, the application of energy spectra analysis has been considered. In the case of structural analysis, due to limited computational resources and the level of detail in the assembly, a convergence analysis was not carried out. Consequently, an interesting alternative for evaluation based on vibrational and resistance criteria through FEM simulations is the application of analysis based on Differential Quadrature Methods (DQM). As shown in various studies [41-45], the DQM technique is used to investigate vibration and bending behavior.

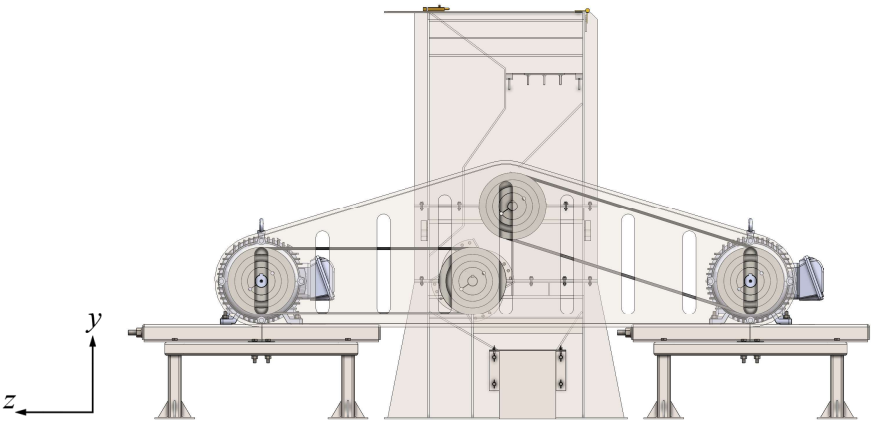

(a)

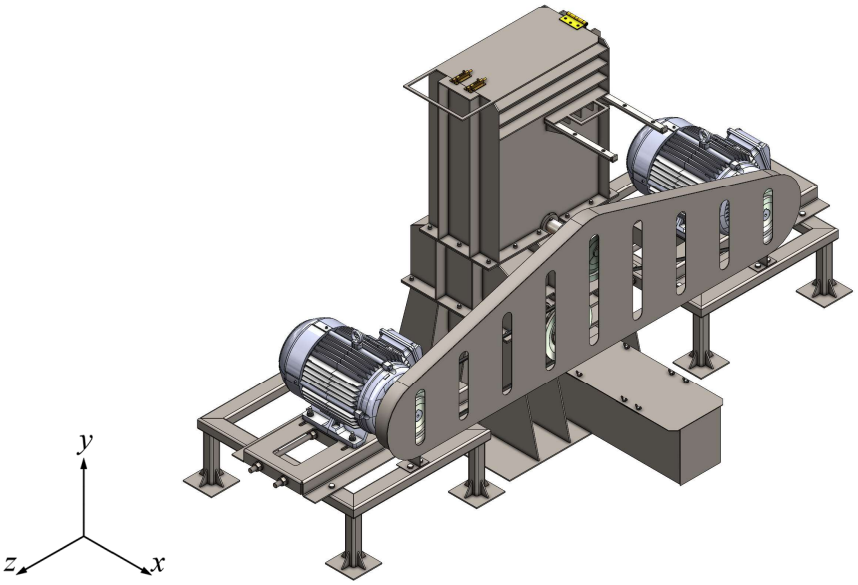

(b)

Fig. 19. "Double rotor impactor" final prototype assembly. (a) Internal View. (b) Isometric view.

(a) (b)

Fig. 20. Double rotor impactor constructed model. (a) Isometric view. (b) Rotor view.

It is necessary to specify that the methodology focuses on obtaining optimized designs for specific functions according to the guidelines of the generated solution concept. The optimal behavior of the prototype lies in its specificity for the intended use. For the equipment presented in the paper, the shapes and dimensions were optimized specifically to generate crushing according to a process involving impact breakage. In this sense, minerals whose breakage or degradation is more efficient under abrasion processes would find limitations specifically in this final prototype. For example, if a piece of equipment with a broader range of applications is desired, the potential design of that equipment can be addressed by the present methodology in the concept generation stage. It would start by establishing a solution concept that encompasses these characteristics; consequently, the shapes and dimensions of a device that allows adaptation to the characteristics through geometry change would be designed. For instance, a device that allows adjusting the gap between the rotors, changing the shape of the rotors, and even making modifications to the internal geometry.

This research can be understood as the first phase of a comprehensive design process, as it is focused on determining optimal shapes and designing mechanical components of the device. Consequently, the research presents limitations in terms of test scenarios, i.e., the number of prototypes analyzed. There are also limitations regarding the lack of analysis of complementary systems, such as control systems for real-time performance analysis and safety. Additionally, the research has not addressed the analysis and implementation of methodologies for equipment maintenance. However, all these features could be integrated into future work.

Based on this, it is possible to expand the methodology to obtain a more comprehensive and sophisticated final prototype. This research can be enhanced by analyzing more prototypes, based on different comminution generation criteria, such as abrasion, and even by conducting analyses of bio-inspired prototypes. In the future, it would also be possible to implement control systems for vibration analysis, wear, among other necessary implementations to ensure long-term reliability. Additionally, the methodology could integrate more features to address the objectives and principles of a circular economy.

Finally, based on all of the above, this work has sought to promote the attention of the Peruvian industry in the search for efficient alternatives for a responsible mining process. The authors consider that the approach presented is an interesting step towards this objective.

4. Conclusion

The design of a new comminution equipment was conducted utilizing the presented design methodology, which revolves around proposing and testing various equipment prototypes to obtain a final prototype optimized according to the selected solution concept. As a result, shapes and dimensions correspond to a specific design for the crushing function via an impact rotor. The methodology divided into four stages, begins by establishing a conceptual solution, which involves identifying needs, translating these needs into specifications, delineating the process by establishing subfunctions, and ultimately selecting solutions for these subfunctions. Subsequently, to enhance the equipment's efficiency, propose shapes that are evaluated based on predefined characteristics of the concepts. A series of computational simulations employing DEM analysis provide a suitable framework to assess the potential of these shapes. To finally, carry out a structural safety analysis applying FEM simulations.

The methodology has allowed the analysis of the component shapes and internal geometry necessary for optimal equipment. The aim was to have a geometry focused on promoting efficient contact between particles and the rotor blades, as well as to achieve an optimized flow of particles inside the equipment. Through the use of the methodology, it was noted that the top feed facilitated more efficient collisions of particles toward the rotors, maximizing exploitable collisions. Additionally, rotor designs with larger flat areas and some inclination in the blades were found to promote better particle impacts. Furthermore, optimal arrangements of internal components were identified to prevent obstructions and ensure efficient flow among rotors. With this configuration, limestone particles were reduced from 20 mm to 1.00862 mm in equivalent diameter, resulting in a reduction ratio of 1:19.8. Consequently, a final optimized equipment design based on particle breakdown per impact was obtained. The ability to determine which parameters exert the greatest influence on the optimal performance of the equipment and to assess relevant changes in order to achieve an optimal design accounting as one of the main benefits of the methodology.

The present methodology can be understood as the initial phase of a comprehensive design process, as it focuses on optimizing geometries and calculations of mechanical elements for crushing devices. Consequently, the methodology does not include the implementation of systems for real-time evaluation and control of equipment performance. Future work would allow expanding the methodology to address these limitations by proposing systems for vibration analysis and control, wear, structural damage, among others. Additionally, it's feasible to expand the research scope to explore a broader range of prototypes for the crushing device, taking into account various scenarios and crushing criteria, such as abrasion. In this regard, in subsequent research we will present the design of a bioinspired crushing device.

Author Contributions

R.M.R. Panduro planned the scheme, suggested the experiments, conducted the experiments, examined the theory validation, analyzed the empirical results and wrote the original draft; A. Córdova planned the scheme, suggested the experiments, conducted the experiments, examined the theory validation, performed formal analysis and wrote the final draft; J.L. Mantari planned the scheme, initiated and supervised the project, suggested the experiments, performed formal analysis and performed a critical revision. The manuscript was written through the contribution of all authors. All authors discussed the results, reviewed, and approved the final version of the manuscript.

Acknowledgments

The authors would like to thank 032-FONDECYT-BM-INC.INV for the financial support during the course of this work.

Conflict of Interest

The authors declared no potential conflicts of interest concerning the research, authorship, and publication of this article.

Funding

The authors would like to thank 032-FONDECYT-BM-INC.INV for the financial support during the course of this work.

Data Availability Statements

The datasets generated and/or analyzed during the current study are available from the corresponding author upon reasonable request.

Nomenclature

σ^2	Tavares model parameter that represents the variance of the log-normal distribution of fracture energies	W_{rotor}	Weight of rotor [N]
e_{max}	Tavares model parameter that represents the specific impact energy above which all particles would break in a single impact [J/kg]	W_{pulley}	Weight of pulley [N]

e_{50}	Tavares model parameter that represents the median particle specific fracture energy [J/kg]	F_p	Load due to the tension [N]
e_{min}	Tavares model parameter that represents the minimum specific energy for breakage [J/kg]	d_{pre}	Pre-calculated shaft diameter [mm]
e_∞	Tavares model parameter that should be fitted to experimental data	T	Torsional moment [N.mm]
d_0	Tavares model parameter that should be fitted to experimental data	τ_{tPUL}	Pulsating shear stress of the material shaft [MPa]
d	Shaft diameter [mm]	FS	Safe factor of the shaft
ϕ	Tavares model parameter that should be fitted to experimental data	FS_{fat}	Factor of safety according to the C. Bach fatigue criteria
Υ	Tavares model parameter that represents the damage accumulation	σ_{fAL}	Alternating normal stress of the material shaft
A, b'	Tavares model parameters	σ_v	Equivalent stress [MPa]
P	Power consumption [kW]	α_0	Effort ratio according to C. Bach
w	Angular velocity [rad/s]	C_s	Coefficient for surface finish
M	Resultant momentum at the rotors [N.mm]	C_t	Coefficient for diameter
f_s	Factor of safety corresponding to the operational conditions	C_c	Coefficient for reliability
CD	Separation between the driving and driven shafts [mm]	C_{temp}	Coefficient for temperature
C_θ	Angle of wrap correction factor	M_f	Bending moment at the evaluated zone [N.mm]
C_L	Belt length correction factor	M_t	Torsional moment at the evaluated zone [N.mm]
T_1	Belt slack side tension [N]	β_f	Concentration factor of bending effective stresses
T_2	Belt tight side tension [N]	β_t	Concentration factor of torsional effective stresses
r	Notch radius [mm]	n_k	Notch sensitivity factor according to Thum
R_1, R_2	Reactions of the bearings on the shaft [N]	α_f	Shape factors of notched round bar under bending stress
F_{rotor}	Load of rotor over the shaft [N]	α_t	Shape factors of notched round bar under torsional stress

Abbreviations

DEM	Discrete Element Method	DIC	Digital Image Correlation
FEM	Finite Element Method	CDEM	Continuum-Discontinuum Element Method
CFD	Computational Fluid Dynamics	DQM	Differential Quadrature Methods

References

[1] Wills, B.A., Finch, J., *Wills' mineral processing technology: an introduction to the practical aspects of ore treatment and mineral recovery*, Butterworth-Heinemann, Oxford, 2016.
[2] Napier-Munn, T., Is progress in energy-efficient comminution doomed?, *Minerals Engineering*, 73, 2015, 1-6.
[3] Agarwal, S., Dandge, S.S., Chakraborty, S., Parametric analysis of a grinding process using the rough sets theory, *Facta Universitatis, Series: Mechanical Engineering*, 18(1), 2020, 91-106.
[4] Sarker, B., Chakraborty, S., Parametric study of a CNC turning process using discriminant analysis, *Facta Universitatis, Series: Mechanical Engineering*, 21(2), 2023, 201-222.
[5] Bzinkowski, D., Ryba, T., Siemiatkowski, Z., Rucki, M., Real-time monitoring of the rubber belt tension in an industrial conveyor, *Reports in Mechanical Engineering*, 3(1), 2022, 1-10.
[6] Zdravkovic, M., Korunovic, N., Novel methodology for real-time structural analysis assistance in custom product design, *Facta Universitatis, Series: Mechanical Engineering*, 21(2), 2023, 293-305.
[7] Szucs, H., Vehovszky, B., Possibilities of porous-structure representation–an overview, *Acta Technica Jaurinensis*, 14(4), 2021, 553-576.
[8] Malowany, K., Piekarczuk, A., Malesa, M., Kujawińska, M., Wiech, P., Application of 3D digital image correlation for development and validation of FEM model of self-supporting arch structures, *Applied Sciences*, 9(7), 2019, 1305.
[9] Szalai, S., Dogossy, G., Speckle pattern optimization for DIC technologies, *Acta Technica Jaurinensis*, 14(3), 2021, 228-243.
[10] Ogierman, W., Kokot, G., Analysis of strain field heterogeneity at the microstructure level and inverse identification of composite constituents by means of digital image correlation, *Materials*, 13(2), 2020, 287.
[11] Zhou, H., Gao, H., Feng, C., Sun, Z., Simulation of Hydraulic Fracture Propagation in Fractured Coal Seams with Continuum-discontinuum Elements, *Journal of Applied and Computational Mechanics*, 7(4), 2021, 2185-2195.
[12] Powell, M.S., Morrison, R.D., The future of comminution modelling, *International Journal of Mineral Processing*, 84(1-4), 2007, 228-239.
[13] Cundall, P.A., Strack, O.D., A discrete numerical model for granular assemblies, *Geotechnique*, 29(1), 1979, 47-65.
[14] Mindlin, R.D., Deresiewicz, H., Elastic spheres in contact under varying oblique forces, *Journal of Applied Mechanics*, 20(3), 1953, 327-344.
[15] Walton, O.R., Braun, R.L., Stress calculations for assemblies of inelastic spheres in uniform shear, *Acta Mechanica*, 63, 1986b, 73–86.
[16] Zhu, H.P., Zhou, Z.Y., Yang, R.Y., Yu, A.B., Discrete particle simulation of particulate systems: a review of major applications and findings, *Chemical Engineering Science*, 63(23), 2008, 5728-5770.
[17] Zhu, H.P., Zhou, Z.Y., Yang, R.Y., Yu, A.B., Discrete particle simulation of particulate systems: theoretical developments, *Chemical Engineering Science*, 62(13), 2007, 3378-3396.
[18] Weerasekara, N.S., Powell, M.S., Cleary, P.W., Tavares, L.M., Evertsson, M., Morrison, R.D., Carvalho, R.M., The contribution of DEM to the science of comminution, *Powder Technology*, 248, 2013, 3-24.
[19] Tavares, L.M., A review of advanced ball mill modelling, *KONA Powder and Particle Journal*, 34, 2017, 106-124.
[20] Nordell, L., Potapov, A., Novel comminution machine may vastly improve crushing-grinding efficiency, *Sixth International Conference on Semi-Autogenous High Pressure Grinding Technology (SAG 15)*, Vancouver, BC, Canada, 20–24 September, 2015.
[21] Ketterhagen, W.R., Hancock, B.C., Optimizing the design of eccentric feed hoppers for tablet presses using DEM, *Computers & Chemical Engineering*, 34(7), 2010, 1072-1081.
[22] Scherer, V., Mönnigmann, M., Berner, M.O., Sudbrock, F., Coupled DEM–CFD simulation of drying wood chips in a rotary drum–Baffle design and model reduction, *Fuel*, 184, 2016, 896-904.
[23] Zhao, L., Zhao, Y., Bao, C., Hou, Q., Yu, A., Optimisation of a circularly vibrating screen based on DEM simulation and Taguchi orthogonal experimental design, *Powder Technology*, 310, 2017, 307-317.
[24] Hasankhoei, A.R., Maleki-Moghaddam, M., Haji-Zadeh, A., Barzgar, M.E., Banisi, S., On dry SAG mills end liners: Physical modeling, DEM-based

characterization and industrial outcomes of a new design, *Minerals Engineering*, 141, 2019, 105835.
[25] Nagata, Y., Minagawa, M., Hisatomi, S., Tsunazawa, Y., Okuyama, K., Iwamoto, M., Tokoro, C., Investigation of optimum design for nanoparticle dispersion in centrifugal bead mill using DEM-CFD simulation, *Advanced Powder Technology*, 30(5), 2019, 1034-1042.
[26] Cui, D., Wang, G., Lu, Y., Sun, K., Reliability design and optimization of the planetary gear by a GA based on the DEM and Kriging model, *Reliability Engineering & System Safety*, 203, 2020, 107074.
[27] Cleary, P.W., Delaney, G.W., Sinnott, M.D., Cummins, S.J., Morrison, R.D., Advanced comminution modelling: Part 1–crushers, *Applied Mathematical Modelling*, 88, 2020, 238-265.
[28] Nadutyi, V.P., Tytov, O.O., Kolosov, D.L., Sukhariev, V.V., Influence of particle geometry on the efficiency of operation of quasistatic and inertial disintegrators, *Natsional'nyi Hirnychyi Universytet. Naukovyi Visnyk*, 6, 2020, 21-27.
[29] Jiménez-Herrera, N., Barrios, G.K., Tavares, L.M., Comparison of breakage models in DEM in simulating impact on particle beds, *Advanced Powder Technology*, 29(3), 2018, 692-706.
[30] Cleary, P., Modelling comminution devices using DEM, *International Journal for Numerical and Analytical Methods in Geomechanics*, 25(1), 2001, 83-105.
[31] Tavares, L.M., André, F.P., Potapov, A., Maliska Jr, C., Adapting a breakage model to discrete elements using polyhedral particles, *Powder Technology*, 362, 2020, 208-220.
[32] Ulrich, K.T., Eppinger, S.D., *Product design and development*, McGraw-Hill, New York, 2012.
[33] Nielsen, K., Malvik, T., Grindability enhancement by blast-induced microcracks, *Powder Technology*, 105(1-3), 1999, 52-56.
[34] André, F., Potapov, A., Tavares, L.M., Simulation of single particle breakage using non-Round particles in Rocky DEM, *In 26th International Mining Congress and Exhibition of Turkey*, Antalya, Turkey, 2019.
[35] Gupta, A., Yan, D.S., *Mineral processing design and operations: an introduction*, Elsevier, Amsterdam, 2016.
[36] Mott, R.L., Vavrek, E.M., Wang, J., *Machine elements in mechanical design*, Pearson Higher Ed, New York, 2018.
[37] Budynas, R.G., Nisbett, J.K., *Shigley's Mechanical Engineering Design*, McGraw-Hill, New York, 2011.
[38] Köhler, G., *Maschinenteile: Teil 2*, Teubner, Stuttgart, 1981.
[39] Steinhilper, W., Röper, R., *Maschinen-und Konstruktionselemente 1: Grundlagen der Berechnung und Gestaltung*, Springer, Berlin, 1994.
[40] Steinhilper, W., Röper, R., *Maschinen-und Konstruktionselemente 3: Elastische Elemente, Federn Achsen und Wellen Dichtungstechnik Reibung, Schmierung, Lagerungen*, Springer, Berlin, 1996.
[41] Huang, X., Hao, H., Oslub, K., Habibi, M., Tounsi, A., Dynamic stability/instability simulation of the rotary size-dependent functionally graded microsystem, *Engineering with Computers*, 38(Suppl 5), 2022, 4163-4179.
[42] Al-Furjan, M.S.H., Habibi, M., Ghabussi, A., Safarpour, H., Safarpour, M., Tounsi, A., Non-polynomial framework for stress and strain response of the FG-GPLRC disk using three-dimensional refined higher-order theory, *Engineering Structures*, 228, 2021, 111496.
[43] Al-Furjan, M.S.H., Habibi, M., Ni, J., Jung, D.W., Tounsi, A., Frequency simulation of viscoelastic multi-phase reinforced fully symmetric systems, *Engineering with Computers*, 38(Suppl 5), 2022, 3725-3741.
[44] Al-Furjan, M.S.H., Habibi, M., Shan, L., Tounsi, A., On the vibrations of the imperfect sandwich higher-order disk with a lactic core using generalize differential quadrature method, *Composite Structures*, 257, 2021, 113150.
[45] Al-Furjan, M.S.H., Habibi, M., Rahimi, A., Chen, G., Safarpour, H., Safarpour, M., Tounsi, A., Chaotic simulation of the multi-phase reinforced thermo-elastic disk using GDQM, *Engineering with Computers*, 38, 2020, 1-24.

ORCID iD

R.M.R. Panduro https://orcid.org/0000-0002-3479-4406
A. Córdova https://orcid.org/0000-0002-8321-8544
J.L. Mantari https://orcid.org/0000-0002-3621-3425

How to cite this article: Panduro, R.M.R., Córdova, A., Mantari, J.L. Design Methodology of a Novel Comminution Machine, *J. Appl. Comput. Mech.*, 11(1), 2025, 143-159. https://doi.org/10.22055/jacm.2024.46199.4478